PHYSICAL REVIEW B VOLUME 62, NUMBER 22 1 DECEMBER 2000-II

Effect of sputtering pressure-induced roughness on the microstructure and the perpendicular giant magnetoresistance of Fe/Cr superlattices

M. C. Cyrille,[1] S. Kim,[1] M. E. Gomez,[1,*] J. Santamaria,[1,†] C. Leighton,[1] Kannan M. Krishnan,[2] and Ivan K. Schuller[1]
[1]*Department of Physics, University of California–San Diego, La Jolla, California 92093-0319*
[2]*Materials Sciences Division, National Center for Electron Microscopy, Lawrence Berkeley Laboratory, University of California, Berkeley, California 94720*
(Received 10 July 2000)

We have studied the connection between structure and magnetism of Fe/Cr superlattices as a function of sputtering pressure. To measure the perpendicular giant magnetoresistance, we have fabricated microstructured Fe/Cr pillars embedded in SiO_2 and interconnected with Nb electrodes. Because of the uniform current distribution in the Nb electrodes and the minimization of the superlattice-electrode contact resistance, the method allows a simple and independent measurement of the perpendicular superlattice resistance and giant magnetoresistance. A detailed quantitative structural analysis by x-ray diffraction, transmission electron microscopy, and high spatial resolution electron-energy-loss spectroscopy imaging, was correlated with magnetization and anisotropic magnetotransport properties. Structural characterization of $[\mathrm{Fe}(3\,\mathrm{nm})/\mathrm{Cr}(1.3\,\mathrm{nm})]_{20}$ superlattices indicate that the roughness increases monotonically with pressure. The current perpendicular to the plane giant magnetoresistance was also found to increase with pressure. This is interpreted as arising from an enhanced spin-dependent scattering.

I. INTRODUCTION

Since the discovery of giant magnetoresistance (GMR) in magnetic superlattices,[1] much interesting experimental and theoretical work has been done to understand this phenomenon. The GMR depends on several physical properties: the magnetic structure (via the interlayer exchange coupling), the spin-dependent electronic band structure and the spin-dependent electron scattering.[2–5] Both the magnetic coupling and the spin-dependent scattering are influenced by the superlattices microstructure. The antiferromagnetic magnetization alignment at zero field depends on interlayer coupling and superlattices imperfections like spacer thickness fluctuations (that leads to local changes of the coupling) and magnetic pinholes (that leads to ferromagnetic alignment of parts of the sample). Finally, because the spin-dependent scattering occurs at impurities inside the magnetic layers and at the interfaces, changes of superlattice microstructure (via interfacial roughness, interdiffusion, or pinholes density) will affect both bulk and interface properties and as a consequence, the GMR. Although most of the theoretical and experimental work underscores the importance of interfacial roughness on the GMR magnitude, contradictory experiments have been reported on the effect of interfacial roughness on the current in plane[6,8] (CIP) and current perpendicular to the plane[9] (CPP) GMR. Hence, a detailed structural and magnetic characterization is critical to further understand the origin of the GMR.

We have characterized *quantitatively* interfacial disorder in Fe/Cr superlattices tuned by varying the sputtering pressure (P), using two complementary techniques: low-angle x-ray diffraction (LAXRD), and energy-filtered imaging on cross-section samples in an analytical TEM. The superlattice microstructure was then correlated with their magnetization and current perpendicular to the plane (CPP) GMR. LAXRD and electron-energy-loss spectroscopy (EELS) analysis of $[\mathrm{Fe}(3\,\mathrm{nm})/\mathrm{Cr}(1.3\,\mathrm{nm})]_{20}$ sputter-deposited at Ar pressure (P) varying from 4 to 10 mTorr provide evidence that the roughness is correlated, cumulative (through the superlattice stack) and increases with P. The CPP GMR is also found to increase with P.

II. EXPERIMENTAL DESCRIPTION

Fe/Cr (110) superlattices have been grown by dc magnetron sputtering on Si(100) substrates at room temperature. A 130 nm thick Nb buffer layer was deposited prior to the superlattice deposition for transport measurements purposes. The superlattices structure was thoroughly characterized by low angle x-ray diffraction using a Rigaku rotating anode diffractometer with Cu $K\alpha$ radiation. The specular spectra were fitted with the SUPREX refinement program[10] to estimate the interfacial roughness.

A quantitative structural analysis of the superlattices has been achieved with TEM and high spatial resolution EELS in the cross-sectional geometry taking advantage of the energy filtered imaging technique.[11] Analytical electron microscopy investigations were carried out using a Philips CM20-FEG TEM equipped with a Gatan Imaging Filter, capable of obtaining both electron-energy-loss spectra and energy-filtered images in real time.

Magnetotransport measurements in the CPP geometry are not easily achievable because of the small perpendicular resistance[12,13] of the superlattices, although they allow the deconvolution of the electron scattering occurring in the ferromagnetic bulk from those occurring at the interfaces.[14–16] The experimental setup to measure the CPP GMR in Fe/Cr superlattices using microfabrication techniques is detailed elsewhere.[17] Essentially it consists of fabricating Fe/Cr superlattices which are then processed into $30\times30\,\mu\mathrm{m}^2$ pillars which are isolated electrically by SiO_2 and interconnected in

 ©2000 The American Physical Society

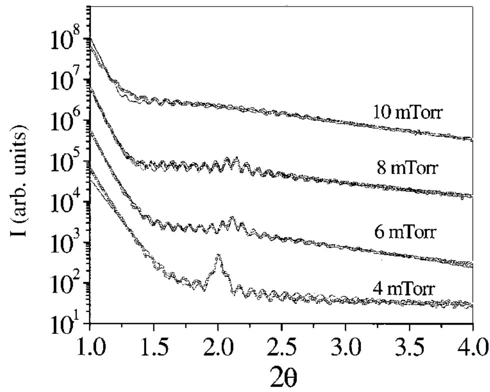

FIG. 1. LAXRD specular spectra taken on a series of superlattices $[\mathrm{Fe}(3\,\mathrm{nm})/\mathrm{Cr}(1.2\,\mathrm{nm})]_{20}$ grown on top of a 100 nm thick Nb buffer layer with sputtering pressures varying between 4 and 10 mTorr. Lines are fits using the SUPREX refinement program. Spectra are offset for clarity.

series with superconducting Nb electrodes. We have estimated the Nb-multilayer contact resistance to be smaller than 0.15 mΩ,[17] while the resistance of our samples is typically more than one order of magnitude bigger. Therefore, because the contact resistance is negligible compared to the actual sample's resistance, no adjustments or corrections have to be done to the measured resistance. The calculated area times contact resistance $2AR_{\mathrm{Nb\ multilayer}}$ (where A is the pillars area) is smaller than 3 $\mathrm{f}\Omega\mathrm{m}^2$.

dc and ac perpendicular magnetotransport measurements were performed in a helium cryostat equipped with a superconducting solenoid. The measurement temperature is 2.0 ± 0.05 K and the applied field is always parallel to the substrate plane.

III. RESULTS AND DISCUSSION

Figure 1 presents the low angle specular x-ray diffraction (LAXRD) spectra taken on a series of superlattices $[\mathrm{Fe}(3\,\mathrm{nm})/\mathrm{Cr}(1.3\,\mathrm{nm})]_{20}$ grown on top of a 130 nm thick Nb buffer layer with sputtering pressures varying between 4 to 10 mTorr.

With the exception of the sample grown at 10 mTorr, all specular spectra exhibit the first superlattice peak and finite size oscillations due to the buffer layer thickness. As P increases, the superlattice Bragg peak broadens and its intensity decreases until it disappears at high pressure, which indicates that the roughness increases with P.[6,10] Note that although the superlattice peak disappears, the overall intensity profile is strongly influenced by the interfacial roughness and will provide structural information.

The surface roughness of sputtered films has been found theoretically and experimentally to scale as a power law of the film thickness t^{α} where α depends on the dynamics of the growth process.[18,19] In superlattices, this type of roughness has been generally modeled as cumulative fluctuations in the layer thickness[10,20,21] or increases in the interface width with increased superlattice thickness.[21] Our structural model assumes a roughness that increases cumulatively with the bilayer index (M) according to a power law $\sigma=\sigma_a M^{\alpha}$ where σ_a is the roughness of the first bilayer, and α an exponent describing the evolution of the roughness.[10] The lines in Fig. 1 are the fit to the data obtained with the SUPREX refinement program.[10]

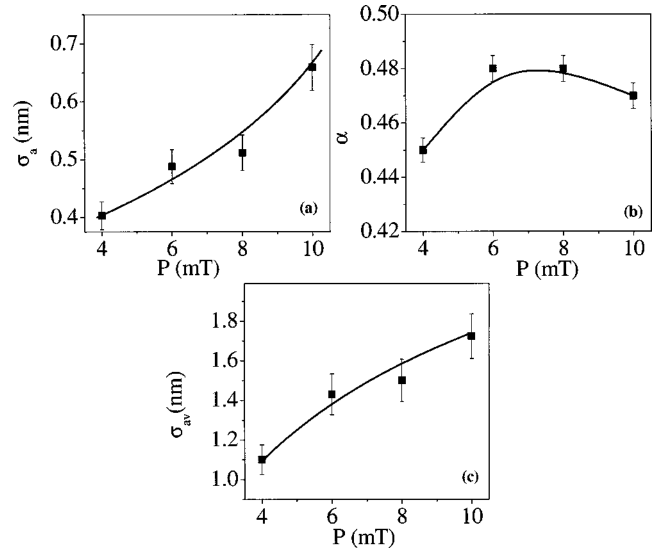

FIG. 2. Roughness parameters (a) σ_a, (b) α, and average roughness (c) σ_{av} as a function of sputtering pressure. Lines are guides for the eye.

The final values of the fitting parameters were checked to ensure they produce minima in the χ^2 confidence factor of the fit. The validity of the cumulative roughness model has been established earlier (using x rays and EELS analysis) for sputtered Fe/Cr superlattices while studying the interfacial roughness as a function of bilayers index.[17] The superlattice modulation length $\Lambda=t(\mathrm{Fe})+t(\mathrm{Cr})$ (where t is the layer thickness), extracted from the fit is in good agreement (within 10%) with nominal values derived from deposition rates. The roughness parameters σ_a and α were extracted from the fits. Figures 2(a) and 2(b) show their evolution with sputtering pressure. Note a significant increase of σ_a with P. A better way to characterize the roughness evolution is to estimate the average superlattice roughness defined by $\sigma_{\mathrm{av}}=\Sigma_{M=1}^{N}\sigma_M/N$ (where M is the bilayer index and N the number of bilayers). As shown in Fig. 2(c), σ_{av} increases monotonically with sputtering pressure.

This is consistent with the increase of roughness reported with P for Fe/Cr superlattices grown directly on Si substrates.[6] It should also be stressed that the presence of the Nb buffer layer introduces some additional roughness. A series of superlattices $[\mathrm{Fe}(3\,\mathrm{nm})/\mathrm{Cr}(1.2\,\mathrm{nm})]_{20}$ was grown on top of Nb buffer layers with thicknesses varying from 0 to 100 nm. Refinement of the low-angle x-ray spectra taken on that series shows a monotonic increase of the roughness parameter σ_a and σ_{av} with the buffer layer thickness.

Quantitative structural analysis of the superlattices has also been obtained with TEM and high spatial resolution energy-filtered imaging in the cross-sectional geometry. Due to the low contrast in scattering power and similar lattice parameters between Fe and Cr, brightfield TEM pictures taken on these samples show only limited diffraction contrast running along the growth direction indicating a columnar growth of the superlattices. On the other hand, EELS pictures showed an enhanced contrast. Cr maps using the $L_{3,2}$ edge ($2p$-$3d$ transitions, following dipole selection rules) of two $[\mathrm{Fe}(3\,\mathrm{nm})/\mathrm{Cr}(1.3\,\mathrm{nm})]_{20}$ superlattices grown on Nb at 4

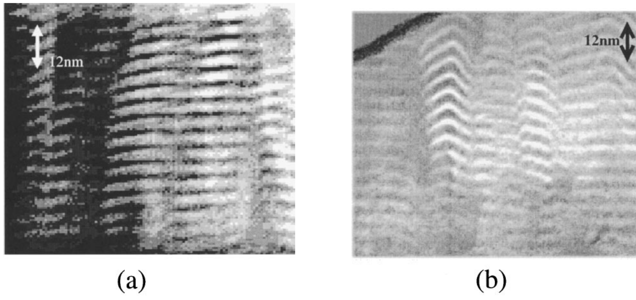

FIG. 3. Cr mapping taken on Nb(130 nm)-[Fe(3 nm)/Cr(1.2 nm)]$_{20}$ grown at (a) 4 mTorr and (b) 10 mTorr.

and 10 mTorr are shown in Figs. 3(a) and 3(b), respectively. Note that the roughness is significantly higher for the sample grown at 10 mTorr and that the roughness is highly correlated. Element (both Cr and Fe) intensity profiles were taken on the same samples along a section perpendicular to the substrate plane with an integration width of 2.7 nm. These profiles were taken every 1.35 nm, along a 100 to 120 nm lateral length (along the multilayer surface). For each Cr (Fe) profile, the position of the maximum EELS intensity was determined. For each bilayer, the roughness is defined as the standard deviation of the Cr intensity maximum over a 100 to 120 nm lateral length.

Figure 4 shows the quantitative roughness as a function of bilayer index for the two superlattices. The lines are fits to the cumulative roughness model ($\sigma=\sigma_a M^{\alpha}$) used to extract the roughness parameters from the LAXRD specular spectra. The first observation is that the roughness increases cumulatively with the bilayer index in both samples as already established for superlattices grown at 5 mTorr.[17] Secondly, not only the roughness of the first layer σ_a increases with P but the roughness progresses much faster at high pressure. The average roughness $\sigma_{av}=\Sigma_{M=1}^{N}\sigma_M/N$ and superlattice modulation length $\Lambda=t(\mathrm{Fe})+t(\mathrm{Cr})$ were extracted for a series of samples sputtered at $P=4$, 6, 8, and 10 mTorr, by measuring the standard deviation of the Cr intensity maxima and the distance between Cr maxima respectively for each individual bilayer. Statistical histograms were plotted and fitted to Gaussian curves to extract the Λ fluctuations. The bilayer thickness fluctuations given by half the FWHM of the Gaussian curves are shown in Fig. 5 together with the average roughness σ_{av} of the superlattice. Figure 5 shows that both

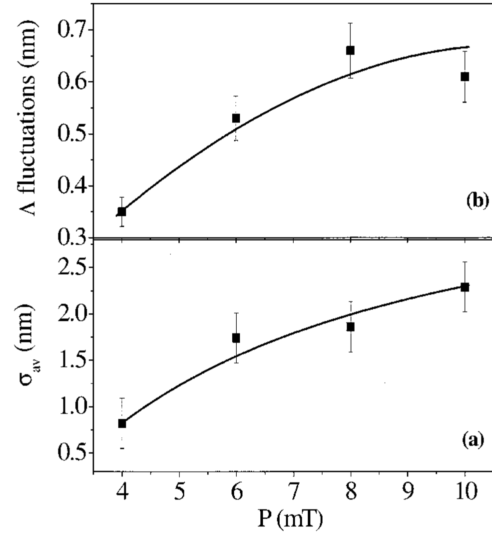

FIG. 5. (a) Average roughness and (b) modulation length fluctuations as a function of P. Lines are guides for the eye.

the average roughness and the bilayer thickness fluctuations increase with pressure. Therefore, *quantitative* EELS analysis confirms the σ_{av} increase with P found from the refinement of the LAXRD spectra.

Magnetization measurements were performed with a SQUID magnetometer at 10 K. Figure 6 presents the dependence of the remnant magnetization (M_R) normalized to the saturation magnetization (M_S) of [Fe(3 nm)/Cr(1.3 nm)]$_{20}$ as a function of P. This quantity gives an estimate of the sample fraction which is not antiferromagnetically aligned at zero field. A small increase of M_R/M_S is observed with increasing P over the 4 to 12 mTorr range. The increase of M_R/M_S can be due to an increased density of ferromagnetic shorts (due to pinholes) between Fe layers, or to Cr thickness fluctuations that can locally change the coupling. Note that the latter would be consistent with the increase of bilayer thickness fluctuations with P as shown by EELS.

A series of [Fe(3 nm)/Cr(1.3 nm)]$_{20}$ superlattices grown at various sputtering pressures was measured in the CPP configuration. The Nb electrodes exhibit a superconducting critical temperature (T_C) of 7.5 K, which is depressed due to degradation during the patterning and the proximity to Fe layers.[22] Below T_C, the 100 pillars in series provide a total

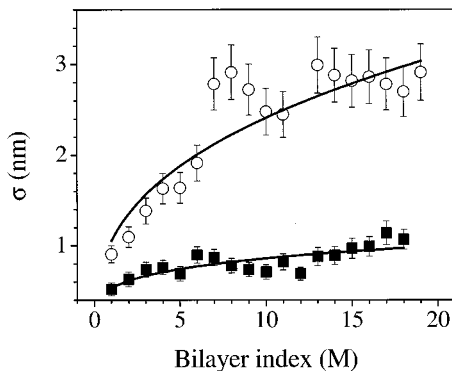

FIG. 4. Roughness of each individual bilayer as a function of the bilayer index M for $P=4$ mTorr (■) and 10 mTorr (○). Lines are fits to the data with ($\sigma=\sigma_a M^{\alpha}$).

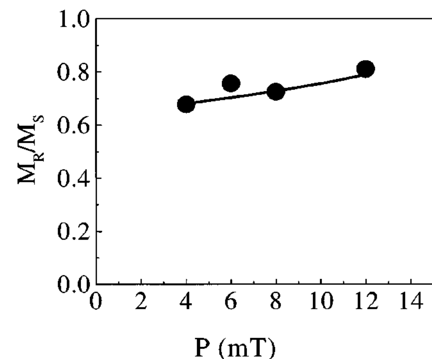

FIG. 6. Remnant magnetization (M_R) normalized to the saturation magnetization (M_S) as a function of sputtering pressure. The line is a guide for the eye.

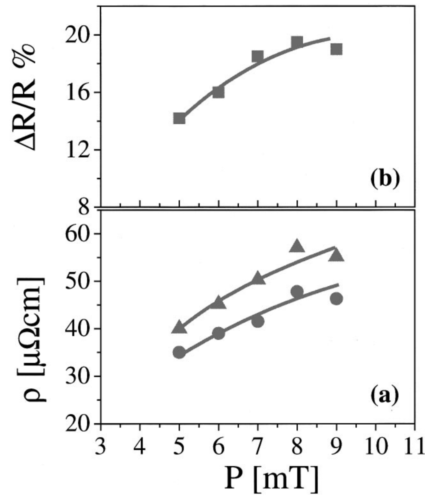

FIG. 7. (a) CPP resistivities ρ_{AP}(▲) and ρ_P(●) as a function of sputtering pressure. (b) CPP GMR ratio (■) as a function of *P*. Lines are guides for the eye.

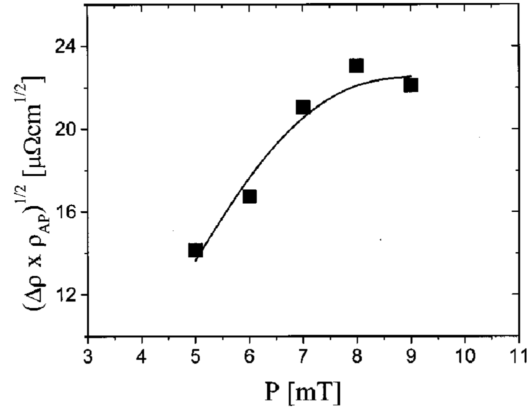

FIG. 8. Plot of $[\Delta\rho\times\rho_{AP}]^{1/2}$ against pressure, *P*, for the CPP data shown in Fig. 7. The solid line is a guide to the eye.

resistance in the mΩ range, which can be measured with conventional techniques. The ''saturation'' field (where ferromagnetic alignment is achieved) is always smaller than the upper critical field of our Nb thin films at 2 K (1.2 T for a 100 nm thick Nb film). It has been shown previously that the contact resistance superlattice-Nb is small compared with the measured superlattice resistance.[17] The uniform current distribution in the superconducting Nb electrodes and the small superlattice-electrode contact resistance assure that the measured resistance is intrinsic.

Figure 7 presents the CPP GMR ratio [defined as $(R_{AP}-R_P)/R_P$] and the perpendicular resistivities ρ_{AP} and ρ_P of $[\mathrm{Fe}(3\,\mathrm{nm})/\mathrm{Cr}(1.3\,\mathrm{nm})]_{20}$ for the two magnetic configurations (antiparallel and parallel alignment). Both the GMR ratio and the resistivities increase with *P*. The GMR increase is due to a faster increase of ρ_{AP} compared to ρ_P. Because the increase of pressure decreases the deposition rate at constant power and changes the surface mobility on the substrate, an increase of resistivity of the same order is expected for ρ_{AP} and ρ_P due to the increased concentration of defects and impurities. This is contrary to what is observed, as ρ_{AP} increases faster than ρ_P.

Note that a loss of antiferromagnetic coupling (due to enhanced contribution of ferromagnetic shorts or Cr thickness fluctuations) is often expected with increasing roughness[6,7] and should decrease the GMR. Figure 6 provides evidence of a small loss of magnetic coupling with pressure-induced roughness. Therefore a decrease of GMR is expected with *P* contrary to what is observed. It should be noted at this stage that our values of M_R/M_S, which reflect the strength of the antiferromagnetic alignment between *F* layers, are somewhat higher than those reported for systems with higher GMR values (e.g., Ref. 13). This would seem consistent with the fact that perfect antiferromagnetic alignment would lead to the maximum GMR values. We therefore note that the specific behavior of the roughness dependence of the GMR may be different in samples with very different tendency to antiferromagnetic alignments.

The enhancement of CPP GMR is the result of a competition between an increase of GMR (due to roughness) and a decrease of GMR (due to the small loss of coupling), the GMR increase being large enough to compensate the effects due to the loss of coupling.

It has been shown theoretically[4] that the CIP GMR of epitaxial Fe/Cr superlattices increases when the step density at the interfaces increases (in the form of a decreased roughness lateral coherence length) or when the step height (vertical roughness) increases. On the other hand, both an increase and decrease of CIP GMR have been reported for polycrystalline Fe/Cr superlattices with roughness induced via annealing, changes of substrate temperature or sputtering pressure.[6–8] A GMR enhancement can be attributed to an increased spin-dependent scattering, a decreased spin-independent scattering or a combination of both. Similarly, a GMR reduction can be due to a decreased spin-dependent scattering, an increased spin-independent scattering or both.

The GMR effect can be explained qualitatively and quantitatively by taking into account a spin asymmetry of the parameters describing the transport properties of the two spin channels, up (↑) and down (↓) for electronic conduction.[14,15] The CPP geometry permits a quantitative analysis of the GMR in terms of interface resistance $R_{F/N}\uparrow(\downarrow)=2R^*_{F/N}(1-(+)\gamma)$ and bulk resistivities of the ferromagnetic layers $\rho_F\uparrow(\downarrow)=2\rho^*_F(1-(+)\beta)$ and of the nonmagnetic layers $\rho_N\uparrow(\downarrow)=2\rho^*_N$. β and γ are the spin asymmetry coefficients from bulk and interface scattering respectively, $R^*_{F/N}$ is the spin averaged interface resistance, ρ^*_F and ρ^*_N are the spin averaged resistivities for the ferromagnetic and nonmagnetic metal, respectively. In the limit where the layer thicknesses are smaller than the spin diffusion lengths in both metals, a series resistor model has been theoretically proposed.[15] This was extensively used (see Refs. 9, 16 and references within) to extract spin asymmetry coefficients and interface and bulk resistivities from CPP data in various systems. Using the Valet and Fert notations, R_{AP} and R_P can be written as follows:

$$AR_{AP}=2AR_{Nb/F}+N\rho^*_F t_F+(N-1)[2AR^*_{F/N}+\rho_N t_N], \quad (1)$$

$$R_P=R_{AP}-\frac{[N\beta\rho^*_F t_F+2(N-1)\gamma AR^*_{F/N}]^2}{A^2R_{AP}}, \quad (2)$$

where A is the pillar area, N the number of bilayers, $R_{\mathrm{Nb}/F}$ the Nb/Fe interface resistance, and t_N and t_F are the thickness of the nonmagnetic and ferromagnetic layer, respectively. Note that the $N-1$ prefix accounts for the last Cr layer which is superconducting due to proximity to the Nb electrode.

Equation (2) illustrates the spin dependent contribution to the electronic transport and can be rewritten using the spin dependent interface resistance and bulk resistivity definitions:

$$A^2(R_{\mathrm{AP}}-R_P)R_{\mathrm{AP}}=A^2\Delta R\times R_{\mathrm{AP}} =N\left(\frac{\rho_F^{\downarrow}-\rho_F^{\uparrow}}{4}\right)t_F+2A(N-1) \times\left(\frac{R_{F/N}^{\downarrow}-R_{F/N}^{\uparrow}}{4}\right). \tag{3}$$

As shown in Fig. 7, both ΔR and R_{AP} increase with pressure. Note that an increase or decrease in spin-*independent* scattering due to enhanced disorder would affect equally both spin channels and would not affect the right-hand side of Eq. (3) contrary to what is observed. Therefore the increase of $\Delta R\times R_{\mathrm{AP}}$ with P is clear indication of an increase of spin-*dependent* scattering and hence an enhancement of the spin asymmetry of the scattering. This increase is shown in Fig. 8.

Note that to have a quantitative statement on the evolution of the spin asymmetry coefficients with pressure, an extensive and lengthy study must be done to extract all parameters for each pressure investigated.

IV. SUMMARY

We have developed a method to measure the perpendicular magnetotransport in metallic superlattices using microfabrication techniques. Because of the minimization of the contact resistance with the electrodes, high number of pillars in series, and the current uniformity in the structures, the method provides simple and direct independent access to the superlattice perpendicular resistance and magnetoresistance.

CPP GMR of $[\mathrm{Fe}(3\,\mathrm{nm})/\mathrm{Cr}(1.3\,\mathrm{nm})]_{20}$ superlattices was investigated and was found to increase with pressure-induced interfacial roughness. The CPP GMR increase is due to an increased spin-dependent scattering.

ACKNOWLEDGMENTS

This work was supported by the U.S. Department of Energy. J.S. thanks the Foundations Jaime del Amo and Flores Valles for their support. M.E.G. thanks Universidad del Valle and COLCIENCIAS. We thank J. Bass, W. Pratt, and A. Fert for critical and helpful comments.

*On leave from Universidad del Valle, A.A.25360 Cali, Colombia.
†On leave from U. Complutense, 28040 Madrid, Spain.

[1] M. N. Baibich, J. M. Broto, A. Fert, F. Nguyen Van Dau, F. Petroff, P. Etienne, G. Creuzet, A. Friederich, and J. Chazelas, Phys. Rev. Lett. **61**, 2472 (1988).
[2] Y. Asano, A. Oguria, and S. Maekawa, Phys. Rev. B **48**, 6192 (1993).
[3] R. Q. Hood, L. M. Falicov, and D. R. Penn, Phys. Rev. B **49**, 368 (1994).
[4] J. Barnas and Y. Bruynseraede, Phys. Rev. B **53**, 5449 (1996).
[5] P. Zahn, I. Mertig, M. Ritcher, and H. Eschrig, Phys. Rev. Lett. **75**, 2996 (1995).
[6] E. E. Fullerton, D. M. Kelly, J. Guimpel, I. K. Schuller, and Y. Bruynseraede, Phys. Rev. Lett. **68**, 859 (1992); J. M. Colino, I. K. Schuller, V. Korenivski, and K. V. Rao, Phys. Rev. B **54**, 13 030 (1996); M. Velez and I. K. Schuller, J. Magn. Magn. Mater. **184**, 275 (1998).
[7] R. Schad, P. Belien, G. Verbanck, K. Temst, V. V. Moshchalkov, Y. Bruynseraede, D. Bahr, J. Falta, J. Dekoster, and G. Langouche, Europhys. Lett. **44**, 379 (1998); R. Schad, P. Belien, G. Verbanck, C. D. Potter, H. Fischer, S. Lefebvre, M. Bessiere, V. V. Moshchalkov, and Y. Bruynseraede, Phys. Rev. B **57**, 13 692 (1998); R. Schad, P. Belien, G. Verbanck, V. V. Moshchalkov, Y. Bruynseraede, H. E. Fischer, S. Lefebvre, and M. Bessiere, *ibid.* **59**, 1242 (1999).
[8] N. M. Rensing, A. P. Payne, and B. M. Clemens, J. Magn. Magn. Mater. **121**, 436 (1993).
[9] W. C. Chiang, W. P. Pratt, Jr., M. Herrold, and D. V. Baxter, Phys. Rev. B **58**, 5602 (1998).
[10] I. K. Schuller, Phys. Rev. Lett. **44**, 1597 (1980); W. Sevenhans, M. Gijs, Y. Bruynseraede, H. Homma, and I. K. Schuller, Phys. Rev. B **34**, 5955 (1986); E. E. Fullerton, I. K. Schuller, H. Vanderstraeten, and Y. Bruynseraede, *ibid.* **45**, 9292 (1992); D. M. Kelly, E. E. Fullerton, J. Santamaria, and I. K. Schuller, Scr. Metall. Mater. **33**, 1603 (1995).
[11] R. Rennekamp, J. Thomas, B. Arnold, and K. Suenaga, Fresenius J. Anal. Chem. **361**, 621 (1998).
[12] W. P. Pratt, Jr., S.-F. Lee, J. M. Slaughter, R. Loloee, P. A. Schroeder, and J. Bass, Phys. Rev. Lett. **66**, 3060 (1991).
[13] M. A. M. Gijs, S. K. J. Lenczowski, and J. B. Giesbers, Phys. Rev. Lett. **70**, 3343 (1993).
[14] S. Zhang and P. M. Levy, J. Appl. Phys. **69**, 4786 (1991).
[15] T. Valet and A. Fert, Phys. Rev. B **48**, 7099 (1993).
[16] S.-F. Lee, Q. Yang, P. Holody, R. Loloee, J. H. Hetherington, S. Mahmood, B. Ikegami, K. Vigen, L. L. Henry, P. A. Schroeder, W. P. Pratt, Jr., and J. Bass, Phys. Rev. B **52**, 15 426 (1995).
[17] M. C. Cyrille, S. Kim, M. E. Gomez, J. Santamaria, K. M. Krishnan, and I. K. Schuller (unpublished).
[18] M. Kardar, G. Parisi, and Y. Zhang, Phys. Rev. Lett. **56**, 889 (1986).
[19] H. You, R. P. Chiarello, H. K. Kim, and K. G. Vandervoort, Phys. Rev. Lett. **70**, 2900 (1993).
[20] A. P. Payne and B. M. Clemens, Phys. Rev. B **47**, 2289 (1993).
[21] E. E. Fullerton, J. Pearson, C. H. Sowers, S. D. Bader, X. Z. Wu, and S. K. Sinha, Phys. Rev. B **48**, 17 432 (1993).
[22] G. Verbanck, C. D. Potter, V. Metlushko, R. Schad, V. V. Moshchalkov, and Y. Bruynseraede, Phys. Rev. B **57**, 6029 (1998); Th. Muhge, K. Westerholt, H. Zabel, N. N. Garif'yanov, Yu. V Goryunov, I. A. Garifullin, and G. G. Khaliullin, *ibid.* **55**, 8945 (1997).